Effect of stable stratification on dispersion within urban street canyons: A large-eddy simulation

Citation: Li, Xianxiang, et al. "Effect of stable stratification on dispersion within urban street canyons: A large-eddy simulation." Atmospheric Environment 144 (November 2016): 47-59 © 2016 Elsevier Ltd

As Published: 10.1016/J.ATMOSENV.2016.08.069

Publisher: Elsevier BV

Effect of stable stratification on dispersion within urban street canyons: a large-eddy simulation

Xian-Xiang Li[a,*], Rex Britter[b], Leslie K. Norford[c]

[a] *CENSAM, Singapore-MIT Alliance for Research and Technology, Singapore 138602*
[b] *Department of Urban Studies and Planning, Massachusetts Institute of Technology, Cambridge, MA, USA*
[c] *Department of Architecture, Massachusetts Institute of Technology, Cambridge, MA, USA*

Abstract

This study employs a validated large-eddy simulation (LES) code with high tempo-spatial resolution to investigate the effect of a stably stratified roughness sublayer (RSL) on scalar transport within an urban street canyon. The major effect of stable stratification on the flow and turbulence inside the street canyon is that the flow slows down in both streamwise and vertical directions, a stagnant area near the street level emerges, and the vertical transport of momentum is weakened. Consequently, the transfer of heat between the street canyon and overlying atmosphere also gets weaker. The pollutant emitted from the street level 'pools' within the lower street canyon, and more pollutant accumulates within the street canyon with increasing stability. Under stable stratification, the dominant mechanism for pollutant transport within the street canyon has changed from ejections (flow carries high-concentration pollutant upward) to unorganized motions (flow carries high-concentration pollutant downward), which is responsible for the much lower dispersion efficiency under stable stratifications.
Keywords: Large-eddy simulation (LES), Urban street canyon, Pollutant dispersion, Stable stratification

---

1. Introduction

With the continuous global urbanization process, more and more research interests are directed to the interaction between human activities and the built environment. Special attention is paid to the roughness sublayer (RSL), the region at the bottom of the atmospheric boundary layer (ABL) where the presence of the canopy influences directly the characteristics of the turbulence and dispersion. The RSL extends from the ground to a height of about

*Corresponding author: Dr. Xian-Xiang Li; Singapore-MIT Alliance for Research and Technology (SMART) Centre, 1 CREATE Way, #09-03, Singapore 138602, Singapore; Tel: (65) 6516-2048; Fax: (65) 6684-2118.
Email address: lixx@smart.mit.edu (Xian-Xiang Li)

there times the canopy height and includes the canopy air space (Kaimal and Finnigan, 1994). One of the basic roughness elements in urban areas is the street canyon, a relatively narrow street in-between buildings that line up continuously along both sides. Models of urban street canyons remain the basis of the urban canopy model (UCM) in numerical weather prediction (NWP, e .g., Weather Research and Forecasting model) models to account for the effect of exchange of momentum, heat and scalars between the urban area and overlying atmosphere. It is therefore of practical importance to investigate the flow, turbulence and scalar transport within and above urban street canyons.

The stratification of the atmosphere has great impact on the turbulence and dispersion in urban areas. The nocturnal atmosphere is generally stably stratified, although in urban areas this is sometimes not true due to the urban heat island and strong turbulence. Compared with the convective boundary layer (CBL), theory and observations in the stable boundary layer (SBL) are rather more complex. Turbulence production by shear is counteracted by buoyancy forces, resulting in generally low turbulence levels, or in very stable conditions, intermittent turbulence (van Dop and Axelsen, 2007). The numerical simulation of the SBL is more challenging since the size of turbulent eddies is limited. Therefore, the resolution of the numerical model should be much higher when studying the SBL. Under very stable stratification, turbulence can be intermittent and gravity wave may be generated, which further complicates the problem and makes numerical simulations inapplicable. The numerical simulation using large-eddy simulation (LES) has demonstrated that LES can adequately capture the characteristics of weakly to moderately stably stratified boundary layer (Jiménez and Cuxart, 2005).

Many numerical studies have been conducted for the urban street canyons under unstable and neutral stratification (e. g., Sini et al., 1996; Kim and Baik, 1999; Xie et al., 2006; Li et al., 2008, 2010a, 2012; Dallman et al., 2014; Hang et al., 2016; Cui et al., 2016), while only a few have been done under stable stratification (e. g., Cheng and Liu, 2011b; Xie et al., 2013; Boppana et al., 2014; Li et al., 2015; Tomas et al., 2015). Although stable stratification conditions occur less frequently in urban areas during nighttime than in their rural surroundings due to anthropogenic heat release and the enhanced turbulence by urban structures, the research of stable stratification is still very important from a practical point of view, since the reduced turbulence can lead to strong concentrations of contaminants, and the reduced downward heat flux can result in very low surface temperatures and eventual frost damage in cold regions (Flores and Riley, 2011). Previous research has shown that later at night, when the rural SBL is deeper than the building height, the city is then capped by a stable layer (Godowich et al., 1985). This paper therefore intends to explore the turbulence and dispersion characteristics within urban street canyons under stable stratification, and we will try to investigate the mechanism behind these characteristics, which makes this study distinct from previous studies listed above.

The urban street canyon geometry in this study is essentially a two- dimensional (2D) due to the periodic boundary conditions prescribed in the along-axis direction (see Section 2). According to Vardoulakis et al. (2003) and Li et al. (2006), street canyons might be classified into short ($L/b \leq 3$), medium ($3 < L/b < 7$) and long ($L/b \geq 7$), where L is the street length and b is the street width (see Section 2). When L is infinite, this corresponds to a 2D street canyon; otherwise, a three- dimensional (3D) street canyon geometry must be considered. The flow and pollutant dispersion in 3D urban-like models with thermal effects or under neutral stratification have been investigated in the literature (e. g., Santiago et al., 2014; Hang et al., 2015).

The rest of the paper will be organized as follows. The numerical method and simulation setup will be described in Section 2. Section 3 will present the results of turbulence and pollutant dispersion, followed by a conclusion in Section 4.

2. Methodology

This study employs the LES code (Li et al., 2010a, 2012) developed for incompressible turbulent flow based on a one-equation subgrid-scale (SGS) model.

2.1. Governing equations

The equations for the evolution of the filtered velocity field are derived from the Navier-Stokes equations for incompressible flow, with the buoyancy effect taken into account by Boussinesq approximation. The reference length scale h (the building height of the street canyon), the reference velocity scale U (free-stream velocity) and the reference temperature θ_a (the ambient temperature) are used to make the governing equations dimensionless. The dimensionless, filtered (resolved-scale) conservation equations for momentum, heat and mass read, respectively

$$\frac{\partial \overline{u}_i}{\partial t} + \frac{\partial \overline{u}_i \overline{u}_j}{\partial x_j} = -\frac{\partial \pi}{\partial x_i} - \frac{\partial P}{\partial x_i}\delta_{i1} - \frac{\partial \tau_{ij}}{\partial x_j} + \frac{1}{Re}\frac{\partial^2 \overline{u}_i}{\partial x_j \partial x_j} + \frac{gh}{U^2}\overline{\theta}\delta_{i3}, \tag{1}$$

$$\frac{\partial \overline{\theta}}{\partial t} + \frac{\partial \overline{\theta}\overline{u}_i}{\partial x_i} = -\frac{\partial \tau_{\theta i}}{\partial x_i} + \frac{1}{RePr}\frac{\partial^2 \overline{\theta}}{\partial x_i \partial x_i}, \tag{2}$$

$$\frac{\partial \overline{u}_i}{\partial x_i} = 0, \tag{3}$$

where

$$\pi = \frac{\overline{p}}{\rho} + \frac{1}{3}e, \qquad \tau_{ij} = \overline{u_i u_j} - \overline{u}_i\overline{u}_j - \frac{2}{3}e\delta_{ij},$$
$$\tau_{\theta i} = \overline{u_i\theta} - \overline{u}_i\overline{\theta}, \qquad e = \frac{1}{2}(\overline{u_i^2} - \overline{u}_i^2),$$

$\overline{u}_i$ is the resolved-scale velocity in the i-th direction, π is the modified pressure normalized by constant density ρ, $-\partial P/\partial x_1$ is the mean streamwise pressure gradient prescribed to drive the atmospheric flow, $\overline{\theta}$ is the resolved-scale (potential) temperature, g is the gravitational acceleration, and δ is the Kronecker delta. The Reynolds number is defined as $Re = Uh/\nu$ and Prandtl number Pr is taken as 0.72. The subgrid-scale (SGS) or residual momentum flux τ_{ij} and heat flux $\tau_{\theta i}$ are modeled using the eddy-viscosity assumption as

$$\tau_{ij} = -2\nu_T\overline{S}_{ij}, \qquad \text{and} \qquad \tau_{\theta i} = -2\nu_\theta\frac{\partial\overline{\theta}}{\partial x_i},$$

respectively, where

$$\overline{S}_{ij} = \frac{1}{2}\left(\frac{\partial\overline{u}_i}{\partial x_j} + \frac{\partial\overline{u}_j}{\partial x_i}\right).$$

The turbulent viscosity for momentum ν_T and diffusivity for heat ν_θ are modeled as $\nu_T = C_k\ell e^{1/2}$ and $\nu_\theta = (1 + 2\ell/\Delta)\nu_T$, respectively, where C_k is a constant (see below), ℓ is the length scale (or filter width), and $\Delta = (\Delta_x\Delta_y\Delta_z)^{1/3}$ is the local grid size.

The transport equation for SGS turbulent kinetic energy (TKE) e reads

$$\frac{\partial e}{\partial t} + \overline{u}_i\frac{\partial e}{\partial x_i} = \mathcal{P} + \mathcal{B} - \varepsilon + \frac{\partial}{\partial x_i}\left(\frac{2}{Re_{\mathrm{T}}}\frac{\partial e}{\partial x_i}\right), \tag{4}$$

where

$$\mathcal{P} = -\tau_{ij}\overline{S}_{ij}, \qquad \mathcal{B} = -g\nu_\theta\frac{\partial\overline{\theta}}{\partial z},$$
$$\varepsilon = C_\varepsilon\frac{e^{3/2}}{\ell}, \qquad Re_{\mathrm{T}} = Uh/\nu_{\mathrm{T}}.$$

The $C_k = 0.03$ and $C_\varepsilon = 1.0$ are model constants (Li et al., 2010b). The length scale ℓ is defined as (Moeng, 1984; Saiki et al., 2000)

$$\ell = \begin{cases} \Delta & \text{for neutral and unstably stratified region,} \\ 0.76\left(\frac{e^{1/2}}{N}\right) & \text{for stably stratified region,} \end{cases} \tag{5}$$

where N is the Brunt-Väisälä frequency defined by $N^2 = \frac{g}{\theta_a}\frac{\partial\overline{\theta}}{\partial z}$.

The conservation equation for pollutant mixing ratio $\overline{c}$ reads

$$\frac{\partial\overline{c}}{\partial t} + \frac{\partial\overline{u}_i\overline{c}}{\partial x_i} = -\frac{\partial\sigma_i}{\partial x_i} + \frac{1}{ReSc}\frac{\partial^2\overline{c}}{\partial x_i\partial x_i} + S, \tag{6}$$

where $\sigma_i = \overline{u_i c} - \overline{u}_i \overline{c}$ is the SGS flux, Sc is the Schmidt number (which is prescribed as 0.72 in this study), and S is the source term. Similarly, σ_i is modeled as

$$\sigma_i = -\nu_c \frac{\partial \overline{c}}{\partial x_i},$$

where $\nu_c = (1 + 2\ell/\Delta)\nu_T$.

The above equations are solved using the Galerkin finite element method. The detailed mathematical formulation of the above equations was discussed in Li et al. (2010b).

2.2. Computational domain and boundary conditions

Figure 1 depicts the schematic computational domain used in the current study, which represents a typical street canyon in an idealized manner. The spanwise-homogeneous computational domain consists of a street canyon of height h at the bottom and a free shear layer of depth $3h$ above the building. The width of the street is b and its length is L. In our study, a street canyon of aspect ratio (AR, h/b) 1 with $h = b = L$ is considered. The inlet and outlet length $b_u = b_d = 0.5b$.

The background atmospheric flow is simulated in the form of a pressure-driven free stream in the free shear layer only. The approaching flow is perpendicular to the street axis, which results in a free-stream wind speed U in the streamwise direction. The air flow boundary conditions are set to be periodic in the streamwise and spanwise directions, and no-slip conditions are set at all rigid walls. At the top of the domain, a shear-free boundary condition ($\partial \overline{u}/\partial z = \partial \overline{v}/\partial z = \overline{w} = 0$, $\partial e/\partial z = 0$) is assumed.

A line source of length L with emission rate Q is located on the ground along the street axis at a distance x_s ($= b/2$ in this study) from the leeward building. At the inlet, the temperature is set to θ_a and pollutant concentration is set to zero (free of pollutant). At the outlet, the convective boundary conditions (Li et al., 2008) are prescribed for both the temperature and pollutant to ensure that they are convected outside the domain and will not enter into the domain again from the inlet. The air temperature at the top is set to the ambient temperature θ_a and the ground level (bottom) maintains a constant temperature $\theta_f = \theta_a + \Delta\theta$. When $\Delta\theta < 0$ the street is cooled and a stable stratification occurs. The temperatures at the rigid walls can either be set to a fixed value (ambient temperature θ_a) or adiabatic (no heat flux at walls); we take the former situation in the present study. The pollutant flux is set to zero at rigid walls (including building walls and roofs).

2.3. Simulation conditions

In this study, three scenarios of thermal stratification (neutral, unstable and stable) will be investigated. The bulk Richardson number, which is used to characterize the stability, is defined as

$$Ri = -\frac{gh}{U^2}\frac{\Delta\theta}{\theta_a}. \tag{7}$$

The values of Ri studied here are -0.1 (unstable), 0 (neutral), 0.1, and 0.188 (stable). The Reynolds numbers based on building height h and free-stream velocity for these cases vary from about 8,000 to 11,000, all above 3000, the critical value for the flow within the street canyon to be independent of the viscosity effect (Hoydysh et al., 1974).

The grid used for the street canyon of AR 1 consists of $128 \times 64 \times 128$ and $256 \times 64 \times 216$ elements inside and above the street canyon, respectively. The grid is stretched near the wall to better resolve the near-wall turbulence. The minimum grid sizes are $2.632 \times 10^{-3}H$ in the streamwise and vertical directions and $1.563 \times 10^{-2}H$ in the spanwise direction. This spatial resolution is about twice higher as those for the neutral (Li et al., 2008, 2009) and unstable stratification cases (Li et al., 2010a, 2012). The distance between the walls and the first grid away from the walls, expressed in wall unit, is about 0.55, which is less than 1, satisfying the requirement for the no-slip condition prescribed along the walls.

The simulation was first performed for neutral stratification condition ($\Delta\theta = 0$) and, when a turbulent flow was established, switched to unstable/stable stratification condition ($\Delta\theta < 0$ or $\Delta\theta > 0$). The time for the flow to reach pseudo-steady state was about $400h/U$. Another $300h/U$ simulation results were collected to retrieve the statistical flow, turbulence, and scalar properties with a time step of $0.0025h/U$, which is half of that used for the above-mentioned neutral and unstable stratification studies.

3. Model validation

The model described in the previous section has been validated against isothermal wind-tunnel data (Li et al., 2010a), and then was validated for an urban street canyon with ground heating (Li et al., 2012). The simulated thin thermal boundary layer near the ground agreed very well with wind-tunnel measurements (Uehara et al., 2000), which was not resolved in studies using RANS models.

To gain more confidence in the LES model under stable stratification, an additional model evaluation exercise is conducted using an experimental database obtained by the Japanese

National Institute for Environmental Studies in an atmospheric diffusion wind tunnel (Uehara et al., 2000). Their experiment was carried out inside a target street canyon within a model building array and the entire wind-tunnel floor was heated, which is not exactly the same as the configuration described in the previous section. For comparison, the boundary conditions for temperature at the outlet in the LES model are changed to periodic. Thus, the thermal energy convected from the outlet enters the domain from the inlet.

Following Uehara et al. (2000), a bulk Richardson number Rb is introduced to quantify the thermal effects, and is defined as

$$Rb = \left(\frac{gh}{U_h^2}\right)\frac{\theta_h - \theta_f}{\theta_a}, \tag{8}$$

where θ_h is the temperature at the roof level, and U_h is the streamwise velocity at the roof level.

The results from our LES for a street canyon of aspect ratio 1 at $Re \approx 8900$ and $Rb = 0.33$ (which is the closest Rb value from a series of numerical experiments) are compared with the experimental data at $Rb = 0.43$ (Fig. 2). It is clear that the agreement between the current LES results and the experimental data is generally good. The well-simulated wind profile indicates adequate grid resolution in the current LES, especially above the street canyon. In previous studies (Li et al., 2008, 2010a), a vertical domain size of $2h$ was used and a large difference was observed between the simulated and measured wind profile above the street canyon. In present study, a domain height of $4h$ is used instead, signifying the impact of the vertical domain size in simulating correctly wind profile. However, the normalized temperature shows much discrepancy both within and above the street canyon (Fig. 2b). The simulated temperature shows quite constant values both within and above the street canyon, while the measured temperature gradually evolves towards the ambient value.

As demonstrated above, the LES reproduces reasonably well the flow and temperature structure in urban street canyons under different stratifications. For the pollutant dispersion, the LES model was validated against wind-tunnel measurement under isothermal conditions and good agreement was also observed (Li et al., 2008). As no experimental data can be found for pollutant dispersion under unstable or stable stratification conditions, no additional validation is performed for pollutant dispersion here. In the upcoming sections, the validated model will be utilized to study in detail the flow, temperature, and pollutant dispersion inside urban street canyons with different atmospheric stability conditions. The boundary condition for temperature at the outlet reverts to the convective type, as described in the previous section.

4. Results and discussions

In this section, the validated model will be used in this section to reveal the flow and pollutant dispersion characteristics in a stably stratified roughness sublayer. In the following discussions, brackets $\langle\rangle$ represent the spanwise and temporal averages of physical properties, while a prime represents the deviation from their averages.

4.1. Flow and Turbulence

Figure 3 depicts the normalized streamwise velocity $< \overline{u} > /U$ in the centerline ($x/b = 0.5$) of the street canyon under different stabilities. The major difference between all the vertical profiles lies within the street canyon ($z/h \leq 1$). The reverse flow ($< \overline{u} > /U < 0$) in the lower street canyon shows strong dependence on Ri: when $Ri < 0$ this reverse flow has a much stronger maximum than that when $Ri = 0$, indicating an enhancement of in-canyon recirculation by unstable stratification (i.e., both vertical and horizontal velocities are strengthened. See Li et al. 2010b); when $Ri > 0$, this reverse flow is weakened and the location of maximum is shifted upward compared with the cases for $Ri \leq 0$. Near the ground ($x/h \leq 0.15$), the streamwise velocities under stable stratifications are close to zero, showing a stagnant region in the vicinity of street. This can be seen more clearly in Figure 4 which shows the streamline under different stratifications. The stagnant areas near the ground are evident and may make the pollutant released from the street level extremely difficult to disperse, as can be seen in later sections. Also shown in Figure 4 are the Reynolds stresses, which demonstrate a strengthened peak near the roof level under unstable stratification, while becoming weaker with increasing Ri. Since Reynolds stress is responsible for the vertical transport of momentum, it is clear that increasing Ri weakens this transport.

The normalised spanwise mean vorticity

$$\omega_y = \frac{h}{U}\left(\frac{\partial < \overline{w} >}{\partial x} - \frac{\partial < \overline{u} >}{\partial z}\right) \tag{9}$$

is shown in Figure 5. In the isothermal case (Fig. 5a), the LES results agree quite well with the spanwise vorticity measured by Caton et al. (2003, Fig. 5a therein). The layer of large negative vorticity at the roof level indicates a strong shear layer there, but under unstable stratification (Fig. 5b), this shear layer becomes weaker. Under stable stratifications (Fig. 5c, and d), the shear layer at the roof level is much stronger and almost covers the whole roof. This characteristic may be the reason for better/worse pollutant removal under unstable/stable stratifications, as will be seen later. Since this shear layer is located where Kelvin-Helmholtz instability occurs (Louka et al., 2000; Letzel et al., 2008), the stable stratification may help promote the growth of this instability.

In the core region in the street canyon, the spiral negative vorticity becomes larger in magnitude under unstable stratifications, confirming the strengthened recirculation. Under stable stratification, the vorticity magnitude is about the same as in the neutral stratification, but the center of the recirculation is shifted towards the upper right corner of the street canyon. Near the bottom, there is a local maximum under neutral stratification that is enhanced under unstable stratification. However, under stable stratifications, this local maximum is lifted to $z/h \approx 0.15$ with a much reduced magnitude. This fact signifies that the stagnant air near the bottom is decoupled from the major vortex in the street canyon, and it will inevitably negatively impact the pollutant dispersion from the line source located in the center at the street level.

4.2. Temperature distribution

The normalized mean temperature $(<\overline{\theta}> - \theta_a)/\Delta\theta$ (Fig. 6) distribution is very similar under different stratifications. As explained by Li et al. (2010a), this is because the turbulent and diffusive heat fluxes are both linearly dependent on resolved-scale temperature gradients in this LES model, except that the diffusivity for heat ν_θ is not constant. Therefore, at pseudo-steady state, the temperature is roughly governed by an elliptic equation. Since the temperature is fixed at the boundary in the cases studied, the solution to the temperature distribution is basically fixed, and the slight variations of the temperature distribution are due to the differences in advection and the non-constant diffusivity for heat ν_θ.

At the lee side of the street canyon (Fig. 6), the normalised temperature is higher than at the windward side, which is a result of the reverse streamwise velocity near the ground. In the core region of the street canyon, the normalized temperature was rather uniform for all Ri. However, it must be noted that, under stable stratifications, $\Delta\theta < 0$ and smaller normalized temperature corresponds to higher $<\overline{\theta}>$. Therefore, $<\overline{\theta}>$ is higher near the windward side than that near the leeward side. Under stable stratifications, with the stagnant air near the street to suppress the turbulent heat transfer, the temperature within the street canyon is expected to get even lower and the stratification becomes more stable. However, this positive feedback often found in SBL is not likely to occur here due to the fixed-temperature boundary conditions used in this study. By fixing the walls' temperature to the ambient temperature, there implicitly exists heat flux from the building walls to the air within the street canyon to maintain this higher temperature.

Under stable stratifications, the vertical gradient of mean temperature near the roof level is much smaller compared with that under unstable stratification, suggesting that the heat transfer between the street canyon and overlying atmosphere decreases with increasing Ri. This will be quantified in Section 4.4.

4.3. Pollutant dispersion

4.3.1. Mean concentration and flux

The normalised mean pollutant concentration fields $<\bar{c}> UHL/Q$ (Fig. 7) for the neutral and unstable stratifications are generally similar, but the magnitude of the mean concentration is markedly less for unstable stratification case inside the street canyon. On the other hand, under stable stratifications, the stagnant air near the street level results in a 'pool' of high-concentration pollutant there. Otherwise, above $z/h \approx 0.15$, the pollutant concentration under stable stratifications distributes quite similarly to that under neutral stratification, in terms of both the spatial pattern and quantity. Table 1 contrasts the average pollutant within the street canyon, and particularly $z/h \leq 0.15$. The average pollutant mass $\int <\bar{c}> U/Q\, dxdz$ within the whole street canyon increases greatly with increasing Ri, with the pollutant mass at $Ri = 0.188$ almost 4 times that at $Ri = -0.1$. More strikingly, at $Ri = 0.188$, the pollutant mass in the lower 15% street canyon takes up almost half of the total pollutant mass within the street canyon.

The vertical pollutant concentration fluxes $< w'c' > (HL/Q)$ for each case are depicted in Figure 8 for comparison to further demonstrate the effect of stratifications. Under neutral stratification, there is a strong vertical flux near the windward wall due to the mixing of the pollutant re-entering the street canyon with pollutant-free air from the free stream. However, under unstable stratification, this vertical flux weakens, and instead the vertical flux in the wake of the line source becomes strengthened and strong vertical fluxes are observed along the leeward wall, which is absent from the neutral stratification. These are speculated to transport more pollutants from the line source to the roof level, which has been confirmed by Li et al. (2010a, 2012). The change by stable stratifications (Fig. 8c, d) is even more prominent. The flux near the leeward wall changes to negative from positive under unstable stratification. This indicates that the turbulent transport of pollutant becomes downward rather than upward, due to the reduced updraft there. In the lower corner near the windward wall, there is a strong local maximum of pollutant flux between the interface of the main vortex and the 'pooling' air near the bottom (see Fig. 8c, d). The magnitude of this maximum is higher than that at the roof level. This shows that there is substantial upward transport of pollutant, due to the slowed downdraft there, which consequently brings less relatively fresh (less polluted) air down. The mechanism of these changes under stable stratifications will be further examined in Section 4.3.2.

With the aforementioned drastic changes of the pollutant flux pattern, the pollutant transport at the roof level is expected to show significant difference under stable stratifications. To verify this, the pollutant concentration budget (by taking the average of the pollutant transport equation (6), see Li et al. 2009)

$$\frac{\partial \langle \overline{c} \rangle}{\partial t} = \underbrace{-\langle \overline{u} \rangle \frac{\partial \langle \overline{c} \rangle}{\partial x}}_{\text{streamwise advection}} \underbrace{-\langle \overline{w} \rangle \frac{\partial \langle \overline{c} \rangle}{\partial z}}_{\text{vertical advection}} \underbrace{-\frac{\partial \langle u'c' \rangle}{\partial x} - \left\langle \frac{\partial \sigma_x}{\partial x} \right\rangle}_{\text{streamwise turbulent transport}} \underbrace{-\frac{\partial \langle w'c' \rangle}{\partial z} - \left\langle \frac{\partial \sigma_z}{\partial z} \right\rangle}_{\text{vertical turbulent transport}} \underbrace{+\frac{1}{ReSc}\left(\frac{\partial^2 \langle \overline{c} \rangle}{\partial x^2} + \frac{\partial^2 \langle \overline{c} \rangle}{\partial z^2}\right)}_{\text{molecular diffusion}} \tag{10}$$

along the roof level for different Ri is compared in Fig. 9. Since the molecular diffusion terms in this equation are negligible, they are not discussed below and shown in Fig. 9.

The pattern of each component of the concentration budget under stable stratification is generally similar to their counterpart under neutral stratification. It is noteworthy that there is a much larger vertical gradient of mean pollutant concentration ($\partial < \overline{c} > /\partial z$) at the leeward side of the roof level under stable stratification. Therefore the vertical advection term has a comparable magnitude under stable stratification to that under neutral stratification, despite that $< \overline{w} >$ under stable stratification is rather small there. On the other hand, the vertical advection under unstable stratification (Fig. 9b) has a large negative contribution to the concentration budget at $0 \leq x/h \leq 0.17$, since $< \overline{w} >$ in that interval is negative (due to a small vortex developing at the upper corner near the leeward building, see Li et al., 2010a), indicating that fresh air is entrained into the street canyon at this leeward corner, which dilutes the pollutant there (Li et al., 2010a). Another notable point is the role of vertical turbulent transport under different stratifications: under unstable stratification, the vertical turbulent transport has a strong positive value at the leeward corner, while under neutral and stable stratifications, this term shows a negative contribution, with the magnitude under stable stratification much larger. This demonstrates the different efficiency of turbulent transport under different stratifications, which deceases with increasing Ri: less high-concentration pollutants are transported to the roof level from the point source by turbulence when the atmosphere becomes more stable.

4.3.2. Turbulence structure of pollutant flux

The turbulence structure (or coherent structure) plays an important role in momentum and scalar transfer processes, and can often be deduced using quadrant analysis. For pollutant flux $w'c'$, the first quadrant (Q1: $w' > 0, c' > 0$) is called ejections, which are the 'ejection' of air with high-concentration pollutant from the urban canyon into the RSL above, while the third quadrant (Q3: $w' < 0, c' < 0$) is called sweeps, which are the replacement of ejected fluid with air of relatively low-concentration pollutant from above the street canyon. These two quadrants contribute positively to the pollutant flux and are called organized motions, while the other two quadrants (Q2: outward interactions, $w' > 0, c' < 0$ and Q4: inward interactions, $w' < 0, c' > 0$) contribute negatively, and are called unorganized motions. These definitions are depicted in Fig. 10. Please note that the definitions of ejections and sweeps here for turbulent pollutant flux are different from those for momentum flux due to the different transport processes of pollutant and momentum. The ratio of turbulent pollutant flux contribution from Q1 and Q3 under different stratifications in the street canyon is presented in Fig 11. Above the street canyon, the ejections dominate regardless of the stability. At the roof level, the contributions from both quadrants are roughly equal, while sweeps contribute slightly higher, which is in accordance with the findings from field measurement of the urban roughness sublayer turbulence (Christen et al., 2007) and other numerical studies (Coceal et al., 2007; Cheng and Liu, 2011a) under neutral stratifications. It is evident that, generally, near the leeward wall the ejections (Q1) dominate, while near the windward wall the sweeps (Q3) dominate, corresponding to the updraft of polluted air and the downdraft of fresh air, respectively. With the increasing Ri, the dominance of Q1 near the leeward wall becomes weaker.

Another important phenomenon observed from Fig. 11 is that, under neutral stratification, there is a region near the leeward corner where Q3 (sweeps) dominates. This region greatly shrinks under unstable stratifications, since the buoyancy enhances the vertical motion there and makes the pollutant transport there much more efficient (see Fig. 8b). Under stable stratifications, this region surprisingly shrinks compared with that under neutral stratification, while we would expect this region to expand due to the reduced pollutant transport by negative buoyancy. Although ejections near the leeward wall seem to dominate under stable stratifications (Fig. 11c and d), the corresponding pollutant fluxes there are negative (see Fig. 8c and d), indicating neither ejections nor sweeps dominate there. To explain these seemingly strange observations, a further check of the ratio of contribution from Q1 and Q4 is performed (Fig. 12) for $Ri = 0.188$. It is evident that, near the leeward wall, the magnitude of Q1 is much lower than that of Q4 (unorganized motions, indicating that flow carries high-concentration pollutant downward, due to the lower-than-average vertical velocity), which actually dominates turbulent pollutant transport there. This signifies that stable stratifications have greatly modified the mechanism of the pollutant transport within the street canyon, resulting in a much worse dispersion efficiency.

4.4. Scalar transfer coefficients

The scalar fluxes from the street canyon are important quantities for the transfer processes between the urban canopy layer and the overlying atmosphere. Mesoscale models or models of urban energy balance require the parameterization of these transfer processes. Therefore, many laboratory and numerical studies have been performed to quantify these processes. If the spatio-temporal average of the scalar flux at the roof level is F and the "strength" of the source is C_s (this can be temperature for heat flux and concentration for pollutant flux), and the ambient (background) "strength" of the scalar is assumed to be zero, the transfer coefficient is then defined as (Barlow et al., 2004; Cai et al., 2008; Cheng and Liu, 2011a)

$$\Phi = F/(UC_s). \tag{11}$$

The exchange velocity is defined as

$$w_T = F/C_s. \tag{12}$$

When F is heat flux and C_s is surface temperature, Φ is often referred to as the Stanton number, St, in the engineering community. Note that here the transfer coefficient is defined for either the air within the street canyon or for a specific facet of the street canyon (e. g., walls, street, and roofs). The scalar emitted from a facet will first be transferred into the air within the street canyon and then be transferred into the RSL. Therefore, three kinds of transfer coefficients can be defined (see, e. g., Cai, 2012): (i) between the RSL and a facet, Φ_{B0}; (ii) between the RSL and the canyon air, Φ_{BC}; and (iii) between a facet and the canyon air, Φ_{0C}. Furthermore, F can be split into parts due to advection and turbulence

$$F^{\text{total}} = F^{\text{adv}} + F^{\text{turb}}, \tag{13}$$

and Φ can also be defined for each part. Previous studies have shown that the transfer coefficients and exchange velocities depend on the urban geometry (e. g., aspect ratio h/b), locations of sources, and atmospheric stability.

Figure 13 shows the transfer coefficients of the passive pollutant from a line source at the street level. Apparently the advective parts of the transfer coefficients are close to 0 for all

Ri for both Φ_{B0} and Φ_{BC}. In addition, Φ_{B0} is generally two orders of magnitude lower than Φ_{BC}, indicating the bottleneck of transfer from the facet to the overlying atmosphere lies in the transfer between the facet and the urban canyon air. Both Φ_{B0} and Φ_{BC} decrease with increasing Ri, with Φ_{BC} declining faster than Φ_{B0}.

Figure 14 shows the transfer coefficients of the active heat (i. e., the heat will interact with and change the flow field, rather than just following the flow field like a passive scalar, e. g., pollutant) from an area source at the street level. Again the transfer due to advection is close to 0 and the transfer due to turbulence overwhelmingly dominates. The most evident difference between Figs. 14 and 13 is that Φ_{B0} for heat is approximately one order of magnitude lower than Φ_{BC}. This shows that the transfer of an active, area source is much more efficient than that of a passive, line source. With increasing Ri, both Φ_{B0} and Φ_{BC} decrease drastically, showing the strong impact of stability on heat transfer.

5. Conclusions

In the present study, a validated large-eddy simulation (LES) code was employed to study the effect of atmospheric stability on the dispersion characteristics within the roughness sublayer (RSL). Four cases with different Richardson numbers, $Ri = -0.1, 0, 0.1, 0.188$ were investigated with very high spatio-temporal resolutions in order to better resolve the small turbulent eddies in stably stratified RSL.

The major effects of stably stratified atmosphere on the flow and dispersion can be summarized as follows.

- The magnitudes of the mean streamwise and vertical velocities within the urban street canyon are lowered. The updraft near the leeward wall and downdraft near the windward wall are both reduced, as well as the reversed flow in the lower half of the street canyon. A stagnant area emerges near the street level, and seems decoupled from the main vortex.
- Under stable stratifications, the vertical gradient of mean temperature near the roof level is much smaller compared with that under unstable stratification. The calculated heat transfer coefficient decreases drastically with increasing stability.
- As a result of the marked changes of flow and turbulence characteristics, the pollutant dispersion exhibits evident differences from that under neutral or unstable stratifications. The pollutant emitted from the street level 'pools' within the lower street canyon, with

about half of the pollutant mass trapped in the lower 15% street at a Richardson number (Ri) 0.188.

- The pollutant concentration flux near the leeward wall becomes negative due to the reduced updraft there. Further quadrant analysis of pollutant concentration flux shows that the dominant mechanism for pollutant transport within the street canyon has changed from ejections (flow carries high-concentration pollutant upward) to unorganized motions (flow carries high-concentration pollutant downward), which causes the much lower dispersion efficiency under stable stratifications.

In summary, the various quantities investigated in this study all pointed to the low efficiency and changing dispersion mechanism under stable stratifications. It was shown that the exchange between the RSL and urban street canyons is strongly dependent on the atmospheric stability. The high near-surface pollutant concentration within street canyons under stable stratifications will increase pedestrians' exposure and exacerbate health issues.

It is worthy noting that the present study simulates the urban flow and dispersion using a low-Reynolds-number model with smooth urban facets, which is different from the realistic scenarios (higher Reynolds number with rough urban facets). While the upscaling of the simulated flow and turbulence characteristics to realistic scenarios is guaranteed by the higher Reynolds number than a critical Reynolds number, the upscaling of simulated scalars (temperature and pollutant concentration) is not well understood yet. In addition, the passive scalar emitted at the road surface is fundamentally different from a real traffic source due to an existing laminar viscous layer between the road surface and the air in the street canyon, which causes a ?bottleneck of transfer? of the pollutant. Therefore, cautions should be taken when interpreting real situations in urban areas according to the model results.

Acknowledgment

This research is supported by the National Research Foundation Singapore under its Campus for Research Excellence and Technological Enterprise programme. The Center for Environmental Sensing and Modeling is an interdisciplinary research group of the Singapore-MIT Alliance for Research and Technology.

References

Barlow, J. F., Harman, I. N., Belcher, S. E., 2004. Scalar fluxes from urban street canyons. Part I: Laboratory simulation. Boundary-Layer Meteorol 113 (3), 369–385.

Boppana, V. B. L., Xie, Z.-T., Castro, I. P., 2014. Thermal stratification effects on flow over a generic urban canopy. Boundary-Layer Meteorol 153 (1), 141–162.

Cai, X., 2012. Effects of differential wall heating in street canyons on dispersion and ventilation characteristics of a passive scalar. Atmos Environ 51, 268–277.

Cai, X.-M., Barlow, J. F., Belcher, S. E., 2008. Dispersion and transfer of passive scalars in and above street canyons—large-eddy simulations. Atmos Environ 42, 5885–5895.

Caton, F., Britter, R. E., Dalziel, S., 2003. Dispersion mechanism in a street canyon. Atmos Environ 37, 693–702.

Cheng, W. C., Liu, C.-H., 2011a. Large-eddy simulation of flow and pollutant transports in and above two-dimensional idealized street canyons. Boundary-Layer Meteorol 139 (3), 411–437.

Cheng, W. C., Liu, C.-H., 2011b. Large-eddy simulation of turbulent transports in urban street canyons in different thermal stabilities. J Wind Eng Industr Aerodyn 99 (4), 434–442.

Christen, A., van Gorsel, E., Vogt, R., 2007. Coherent structures in urban roughness sublayer turbulence. Int J Climatol 27, 1955–1968.

Coceal, O., Dobre, A., Thomas, T. G., Belcher, S. E., 2007. Structure of turbulent flow over regular arrays of cubical roughness. J Fluid Mech 589, 375–409.

Cui, P., Li, Z., Tao, W. Q., 2016. Wind-tunnel measurements for thermal effects on the air flow and pollutant dispersion through different scale urban areas. Build Environ 97, 137–151.

Dallman, A., Magnusson, S., Britter, R., Norford, L., Entekhabi, D.and Fernando, H. J. S., 2014. Conditions for thermal circulation in urban street canyons. Build. Environ 80 (10), 184–191.

Flores, O., Riley, J. J., 2011. Analysis of turbulence collapse in the stably stratified surface layer using direct numerical simulation. Boundary-Layer Meteorol 139 (2), 241–259.

Godowich, J. M., Ching, J. K. S., Clark, J. F., 1985. Evolution of the nocturnal inversion layer at an urban and non-urban location. J Appl Meteorol 24, 791–804.

Hang, J., Lin, M., Wong, D. C., Wang, X. M., Wang, B., Buccolieri, R., 2016. On the influence of viaduct and ground heating on pollutant dispersion in 2D street canyons and toward single-sided ventilated buildings. Atmos Poll Res, DOI:10.1016/j.apr.2016.04.009.

Hang, J., Wang, Q., Chen, X., Sandberg, M., Zhu, W., Buccolieri, R., Di Sabatino, S., 2015. City breathability in medium density urban-like geometries evaluated through the pollutant transport rate and the net escape velocity. Build Environ 94, 166–182.

Hoydysh, W. G., Griffiths, R. A., Ogawa, Y., 1974. A scale model study of the dispersion of pollution in street canyons. APCA paper no. 74-157, 67th Annual Meeting of the Air Pollution Control Association, Denver, Colorado.

Jiménez, M. A., Cuxart, J., 2005. Large-eddy simulations of the stable boundary layer using the standard Kolmogorov theory: Range of applicability. Boundary-Layer Meteorol 115 (2), 241–261.

Kaimal, J. C., Finnigan, J. J., 1994. Atmospheric boundary layer flows: their structure and measurement. Oxford University Press, New York, 289 pp.

Kim, J.-J., Baik, J.-J., 1999. A numerical study of thermal effects on flow and pollutant dispersion in urban street canyons. J Appl Meteorol 38, 1249–1261.

Letzel, M. O., Krane, M., Raasch, S., 2008. High resolution urban large-eddy simulation studies from street canyon to neighbourhood scale. Atmos Environ 42, 8770–9784.

Li, X.-X., Britter, R. E., Koh, T. Y., Norford, L. K., Liu, C.-H., Entekhabi, D., Leung, D. Y. C., 2010a. Large-eddy simulation of flow and pollutant transport in urban street canyons with ground heating. Boundary-Layer Meteorol 137 (2), 187–204, DOI: 10.1007/s10546-010-9534-8.

Li, X.-X., Britter, R. E., Norford, L. K., 2015. Transport processes in and above two-dimensional urban street canyons under different stratification conditions: results from numerical simulation. Environ Fluid Mech 15 (2), 399–417.

Li, X.-X., Britter, R. E., Norford, L. K., Koh, T.-Y., Entekhabi, D., 2012. Flow and pollutant transport in urban street canyons of different aspect ratios with ground heating: Large-eddy simulation. Boundary-Layer Meteorol 142 (2), 289–304.

Li, X.-X., Liu, C.-H., Leung, D. Y., 2010b. Parallel FEM LES with one-equation subgrid-scale model for incompressible flows. Int J Comput Fluid Dyn 24 (1-2), 37–49.

Li, X.-X., Liu, C.-H., Leung, D. Y. C., 2008. Large-eddy simulation of flow and pollutant dispersion in urban street canyons with wall model. Boundary-Layer Meteorol 129 (2), 249–268.

Li, X.-X., Liu, C.-H., Leung, D. Y. C., 2009. Numerical investigation of pollutant transport characteristics inside deep urban street canyons. Atmos Environ 43 (15), 2410–2418.

Li, X.-X., Liu, C.-H., Leung, D. Y. C., Lam, K. M., 2006. Recent progress in CFD modelling of wind field and pollutant transport in street canyons. Atmos Environ 40 (29), 5640–5658.

Louka, P., Belcher, S. E., Harrison, R. G., 2000. Coupling between air flow in streets and the well-developed boundary layer aloft. Atmos Environ 34, 2613–2621.

Moeng, C. H., 1984. A large-eddy-simulation model for the study of planetary boundary-layer turbulence. J Atmos Sci 4 (13), 2052–2062.

Saiki, E. M., Moeng, C.-H., Sullivan, P. P., 2000. Large-eddy simulation of the stably stratified planetary boundary layer. Boundary-Layer Meteorol 95, 1–30.

Santiago, J. L., Krayenhoff, E. S., Martilli, A., 2014. Flow simulations for simplified urban configurations with microscale distributions of surface thermal forcing. Urban Clim 9, 115–133.

Sini, J.-F., Anquetin, S., Mestayer, P. G., 1996. Pollutant dispersion and thermal effects in urban street canyons. Atmos Environ 30, 2659–2677.

Tomas, J. M., Pourquie, M. J. B. M., Jonker, H. J. J., 2015. The influence of an obstacle on flow and pollutant dispersion in neutral and stable boundary layers. Atmos Environ 113, 236–246.

Uehara, K., Murakami, S., Oikawa, S., Wakamatsu, S., 2000. Wind tunnel experiments on how thermal stratification affects flow in and above urban street canyons. Atmos Environ 34, 1553–1562.

van Dop, H., Axelsen, S., 2007. Large eddy simulation of the stable boundary-layer: A retrospect to Nieuwstadts early work. Flow Turb Combust 79 (3), 235–249.

Vardoulakis, S., Fisher, B. E. A., Pericleous, K., Gonzalez-Flesca, N., 2003. Modelling air quality in street canyons: a review. Atmos Environ 37, 155–182.

Xie, X., Liu, C.-H., Leung, D. Y. C., Leung, M. K. H., 2006. Characteristics of air exchange in a street canyon with ground heating. Atmos Environ 40 (33), 6396–6409.

Xie, Z. T., Hayden, P., Wood, C. R., 2013. Large-eddy simulation of approaching-flow stratification on dispersion over arrays of buildings. Atmos Environ 71, 64–74.

Table 1: The time-averaged pollutant mass $\int <\overline{c}> U/Q\, dxdz$ within the street canyon.

Ri	Average pollutant	
	Whole canyon	Lower 15% canyon
−0.1	45.6	10.1
0	89.5	19.6
0.1	145.8	59.6
0.188	187.3	90.0

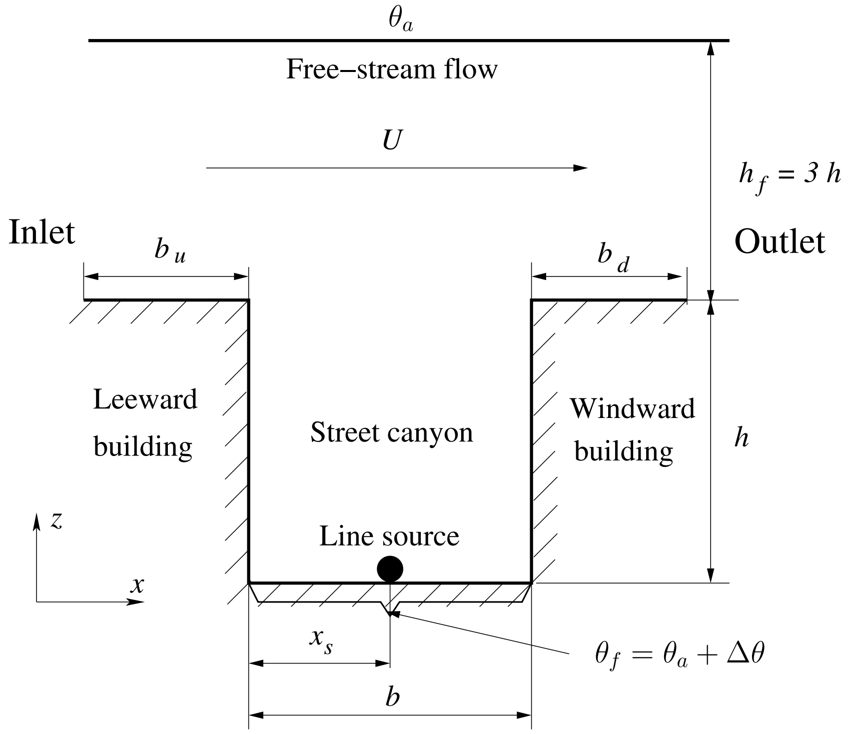

Figure 1: Schematic diagram of computational domain for the flow and pollutant transport in a street canyon.

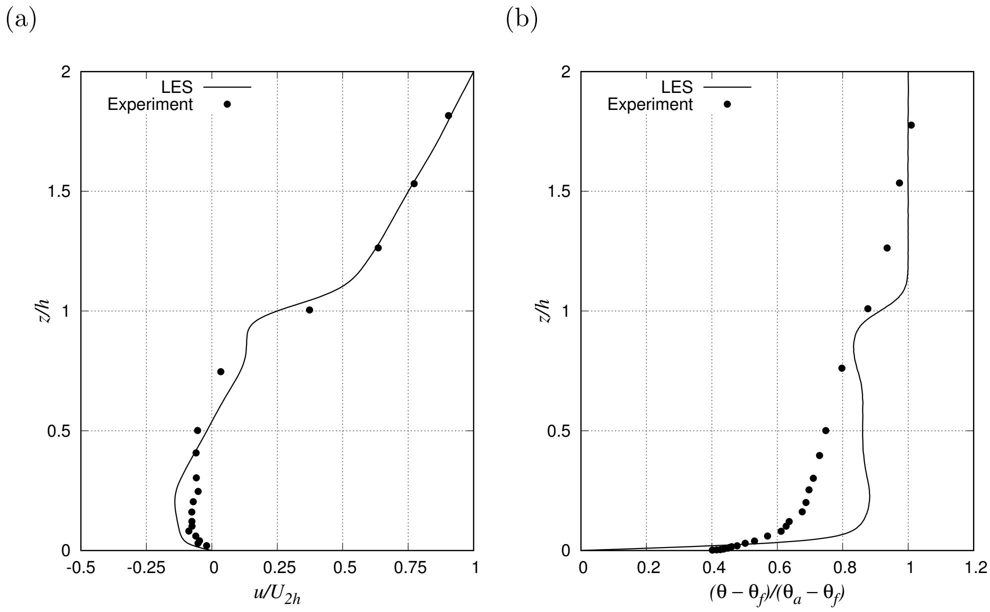

Figure 2: Vertical profiles of normalized (a) average streamwise velocity magnitude $< \overline{u} > /U_{2h}$ and (b) temperature $(< \overline{\theta} > -\theta_f)/(\theta_a - \theta_f)$ along the vertical centreline of the street canyon of aspect ratio 1, where U_{2h} is the average streamwise velocity at $z = 2h$. The experimental data of Uehara et al. (2000) was at $Rb = 0.43$ and the current LES results are at $Rb = 0.33$.

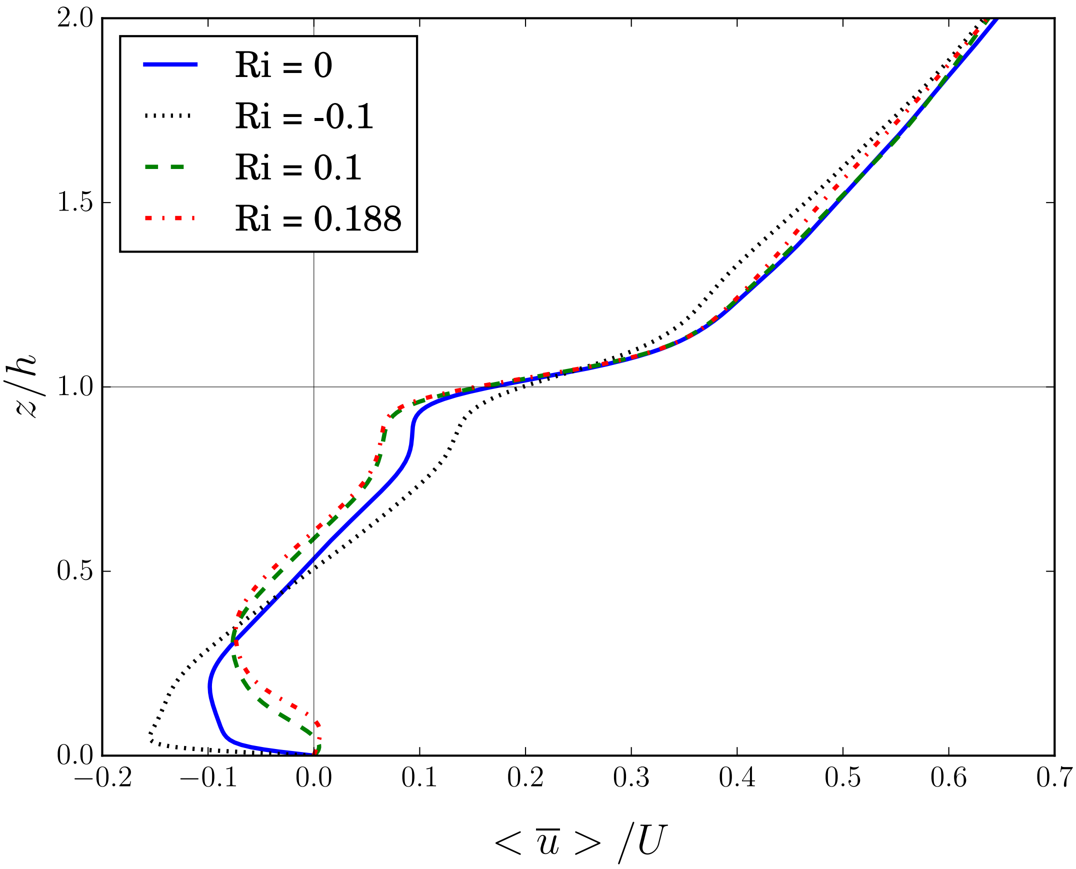

Figure 3: The normalized streamwise velocity in the centerline of the street canyon under different stratifications.

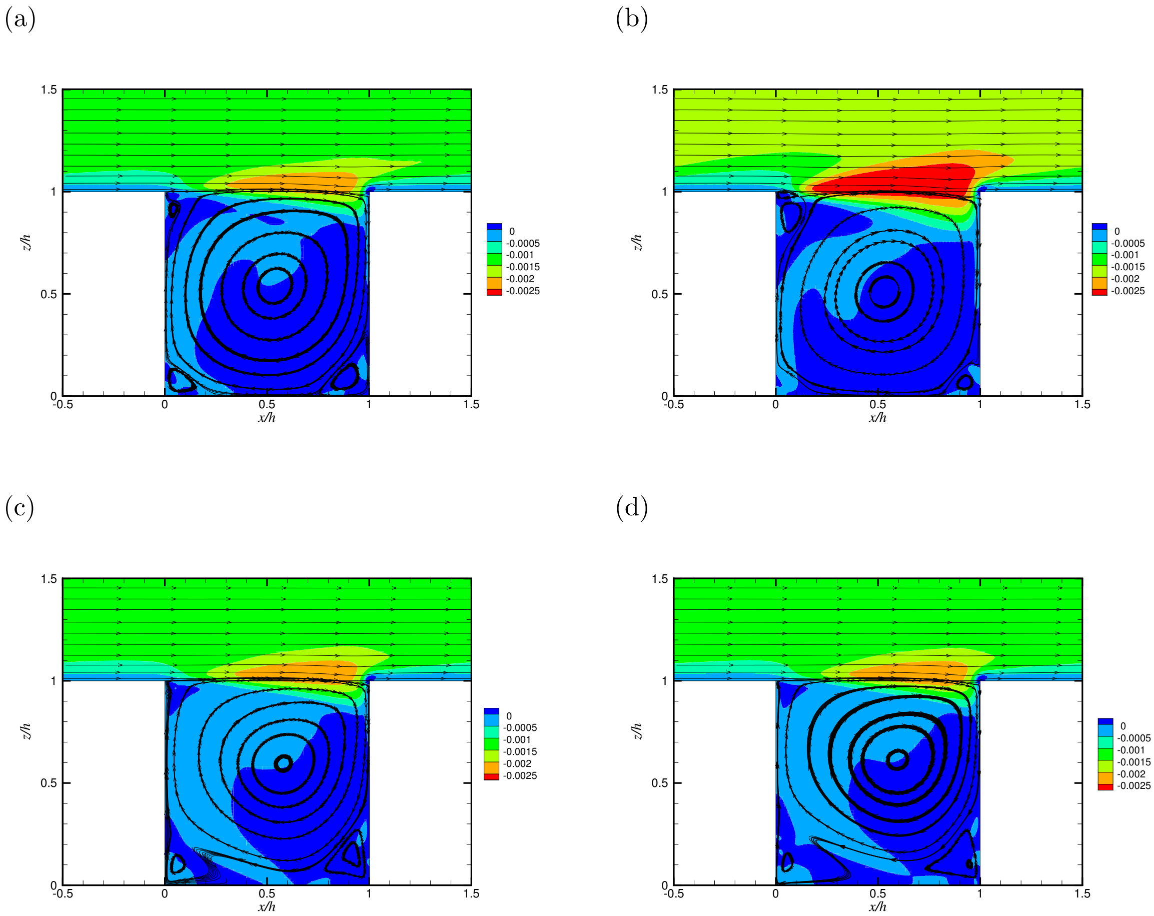

Figure 4: Streamline and normalized Reynolds stress $< u'w' > /U^2$. Ri = (a) 0; (b) -0.1; (c) 0.1; and (d) 0.188.

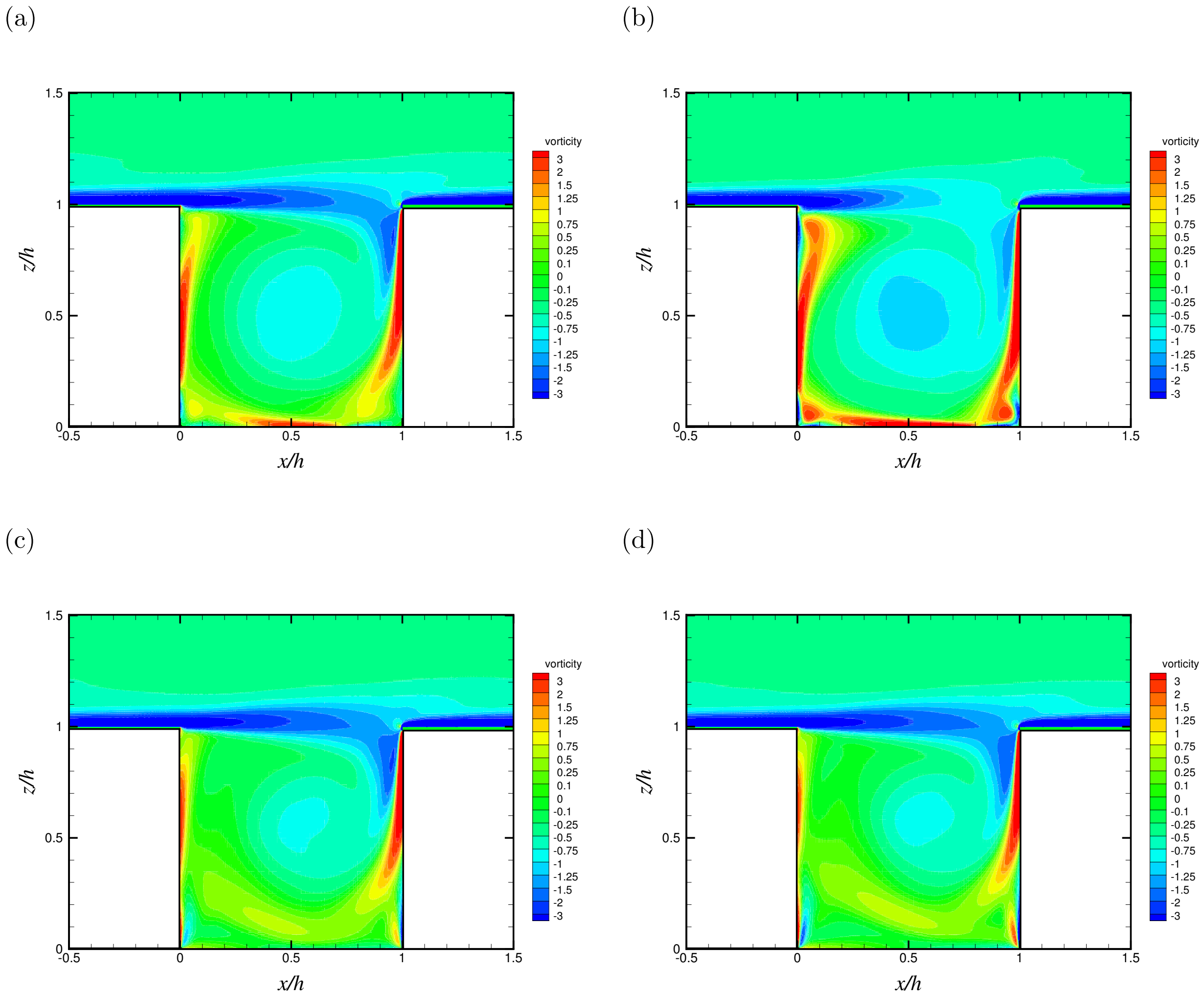

Figure 5: Normalized spanwise vorticity ω_y. Ri = (a) 0; (b) -0.1; (c) 0.1; and (d) 0.188.

(a)

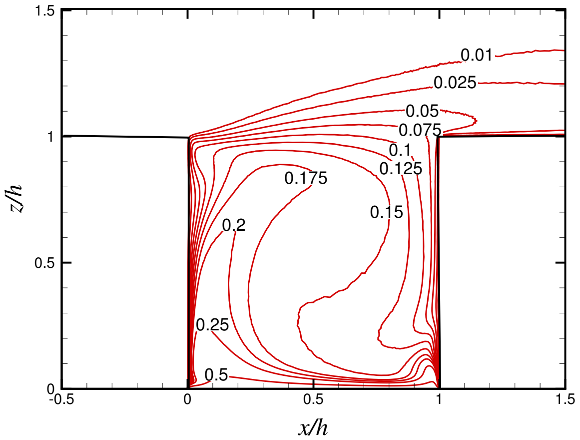

(b)

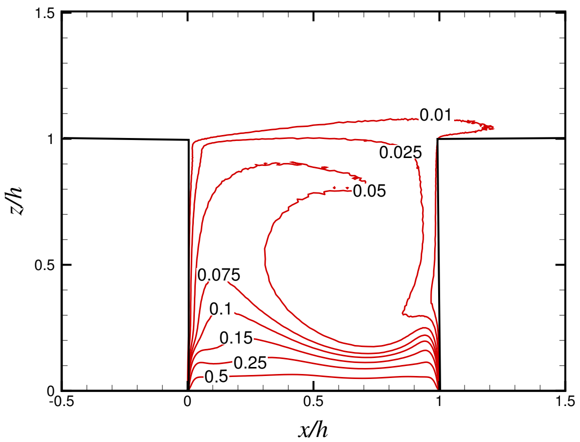

(c)

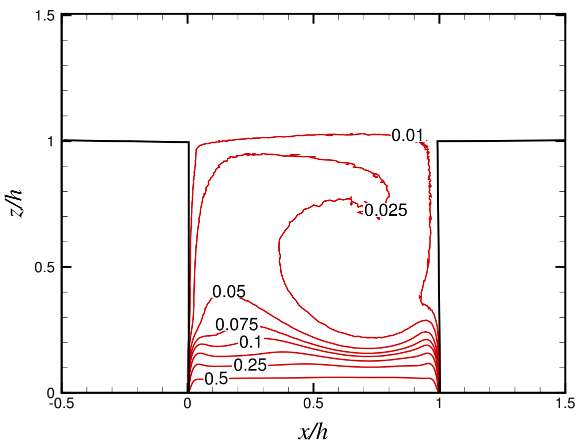

Figure 6: Normalized mean temperature $(<\overline{\theta}> - \theta_a)/(\theta_f - \theta_a)$. Ri: (a) -0.1; (b) 0.1; (c) 0.188.

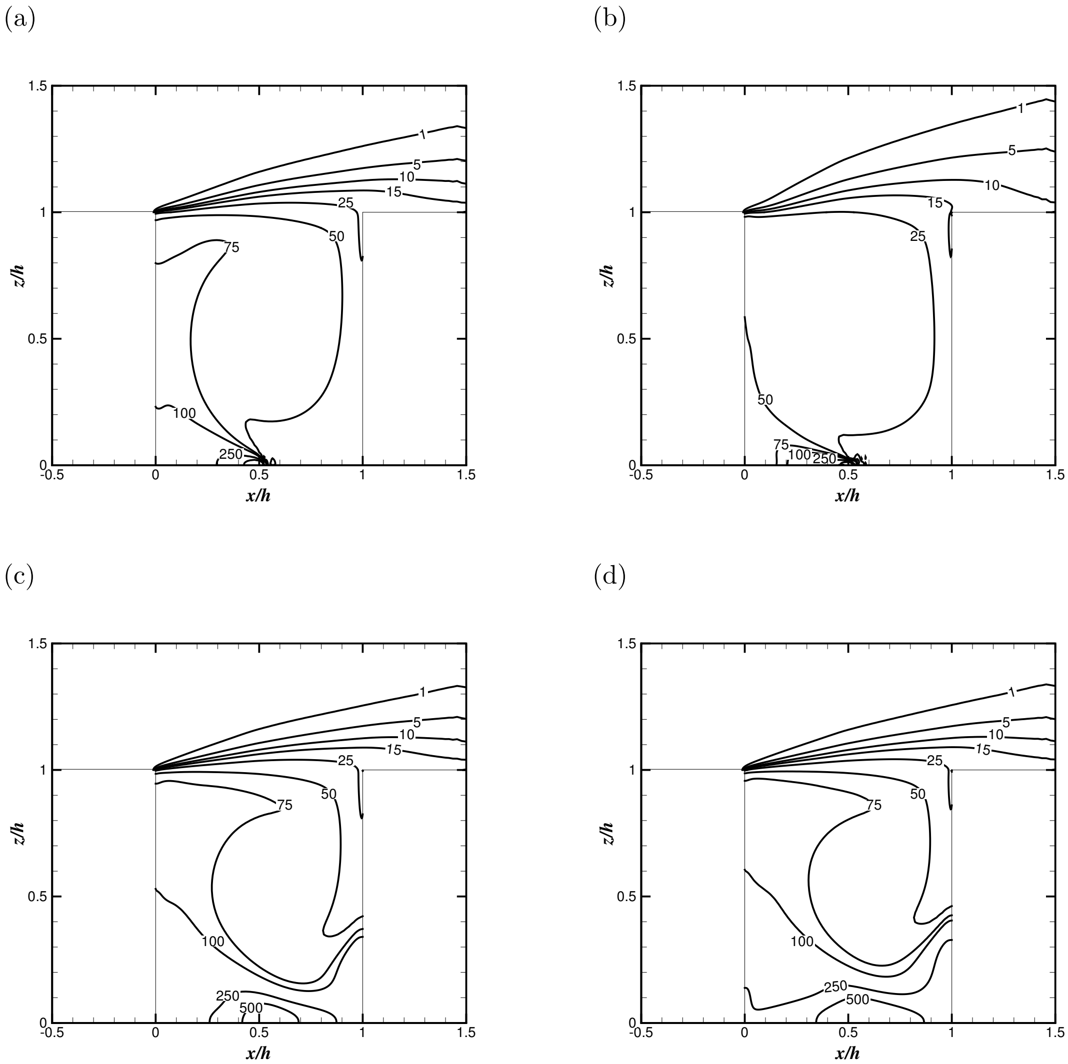

Figure 7: Dimensionless pollutant concentration $<\bar{c}> UhL/Q$. Ri = (a) 0; (b) -0.1; (c) 0.1; and (d) 0.188.

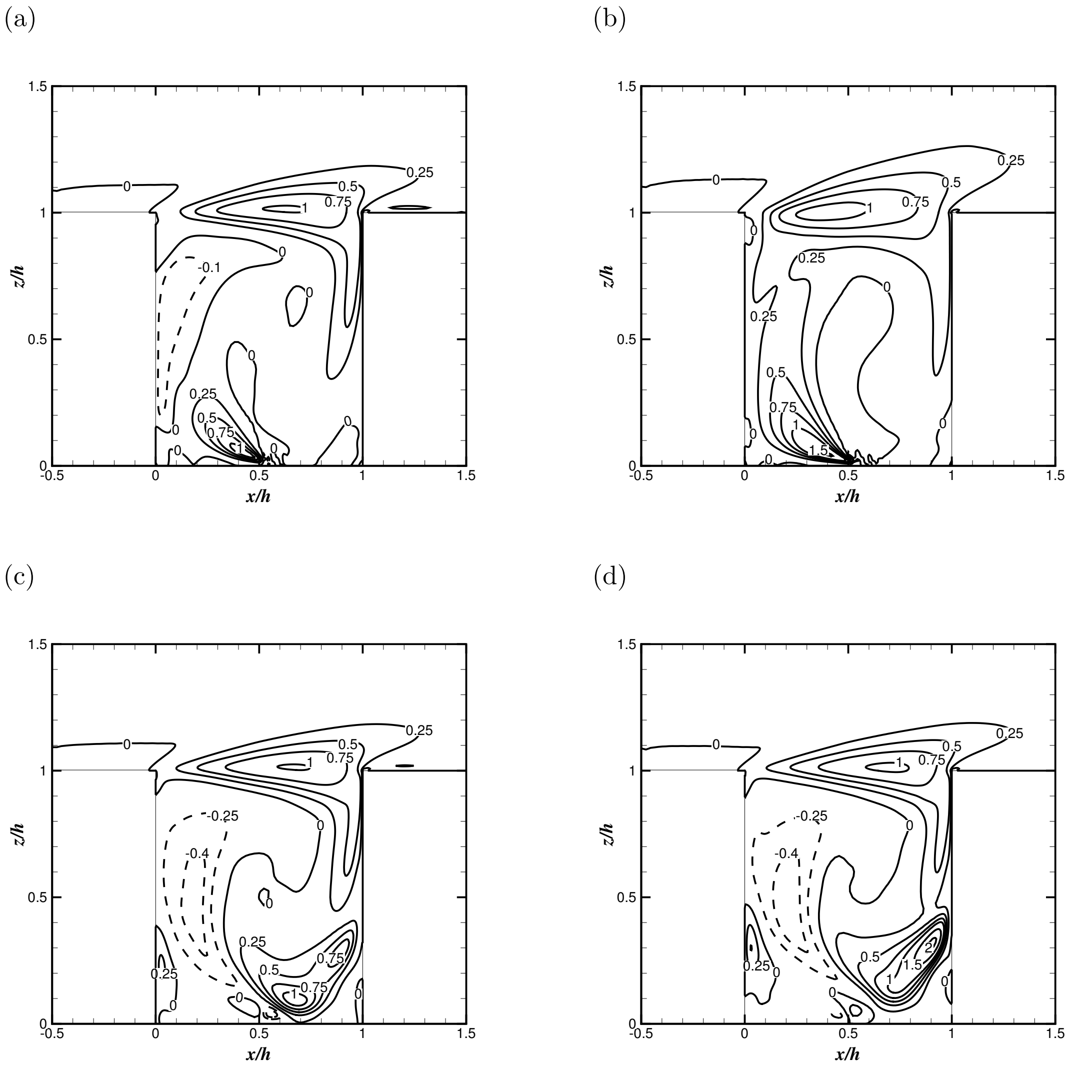

Figure 8: Dimensionless pollutant flux $< w'c' > hL/Q$. $Ri =$ (a) 0; (b) -0.1; (c) 0.1; and (d) 0.188.

(a)

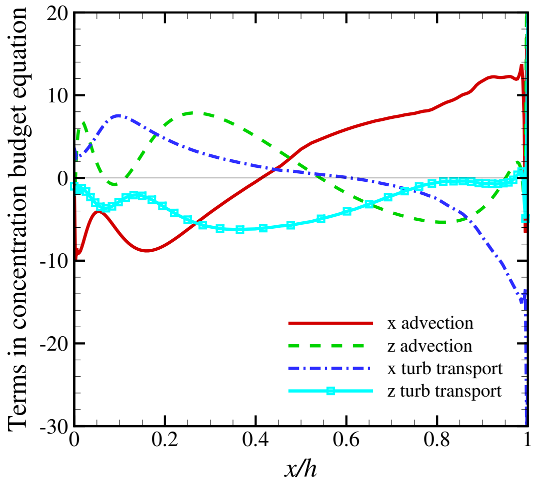

(b)

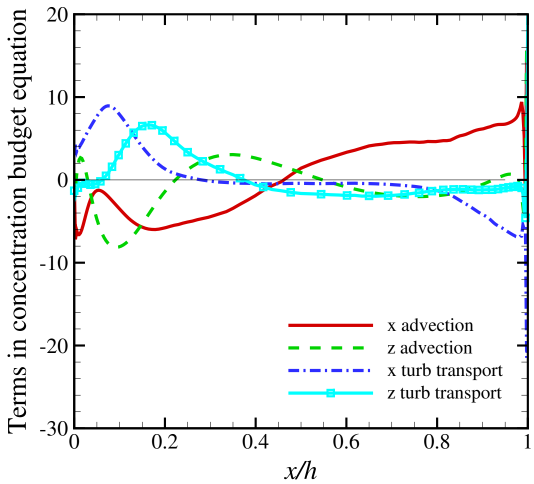

(c)

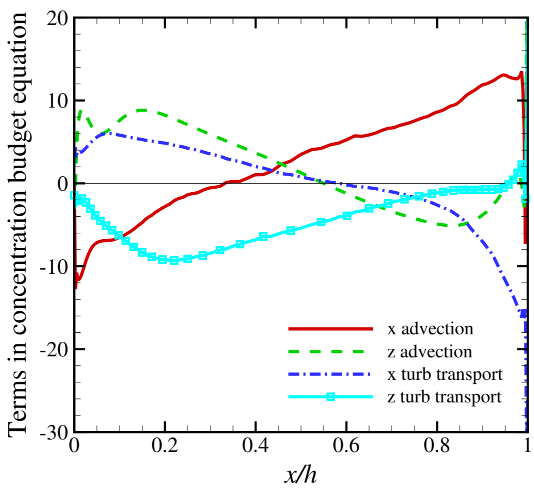

Figure 9: Horizontal distribution of the terms in the normalized pollutant concentration budget equation (10) along the roof level. Ri: (a) 0; (b) -0.1; (c) 0.1.

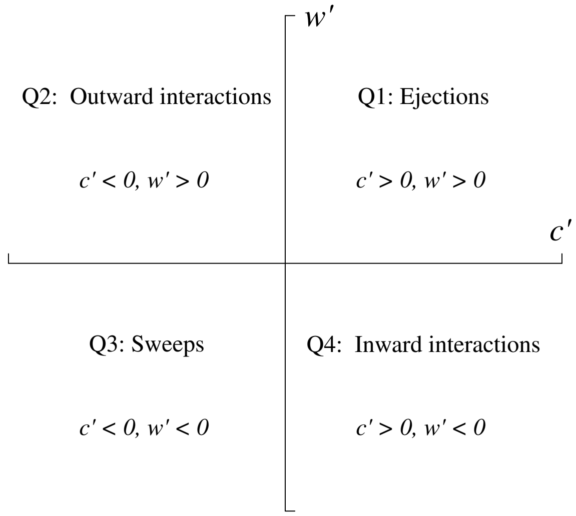

Figure 10: The schematic definitions of quadrants for turbulent pollutant flux.

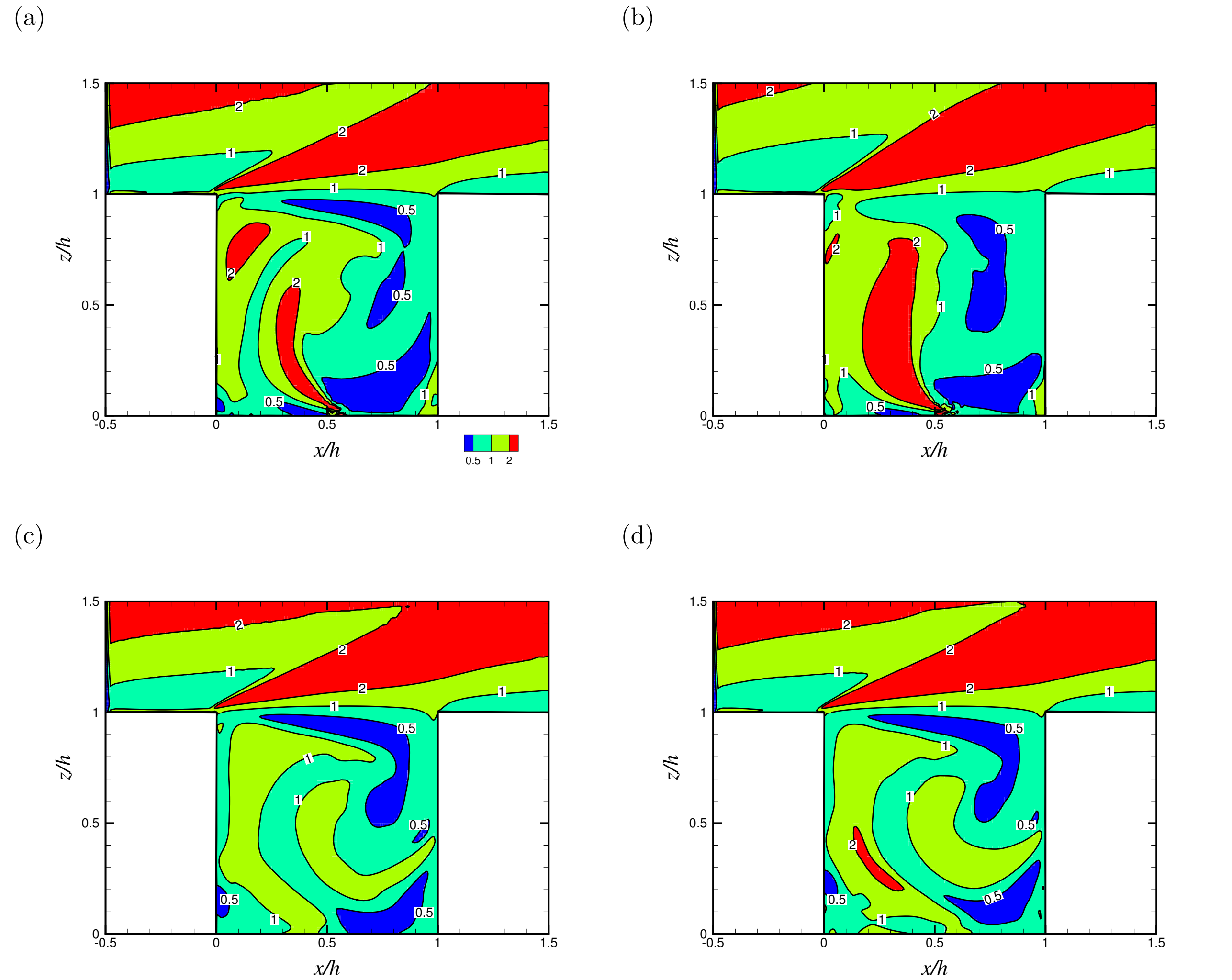

Figure 11: The ratio of pollutant flux contribution from ejections (Q1) and sweeps (Q3). $Ri =$ (a) 0; (b) -0.1; (c) 0.1; and (d) 0.188.

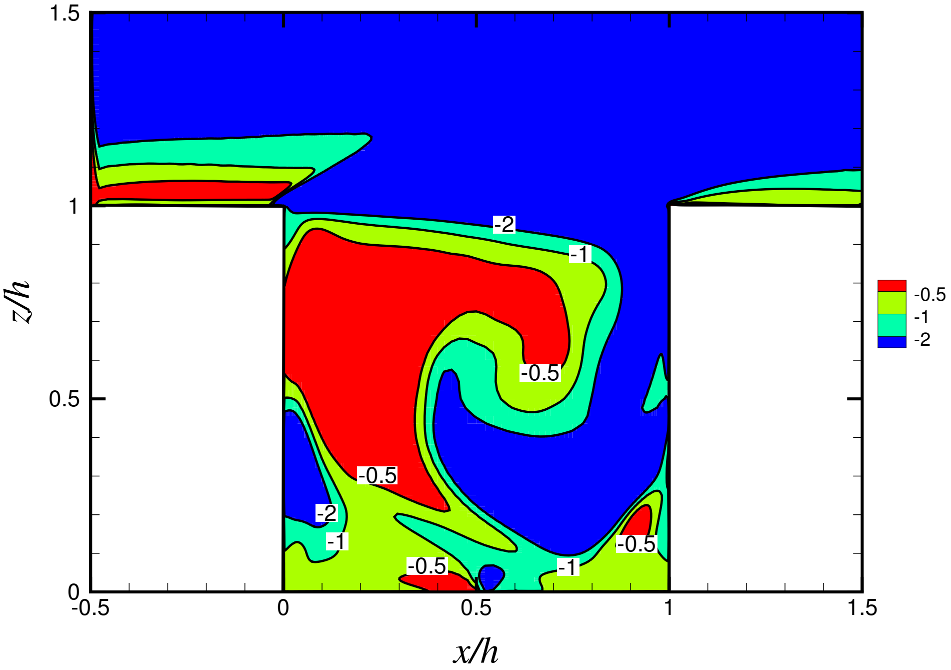

Figure 12: The ratio of pollutant flux contribution from ejections (Q1) and inward interactions (Q4) for $Ri = 0.188$.

(a)

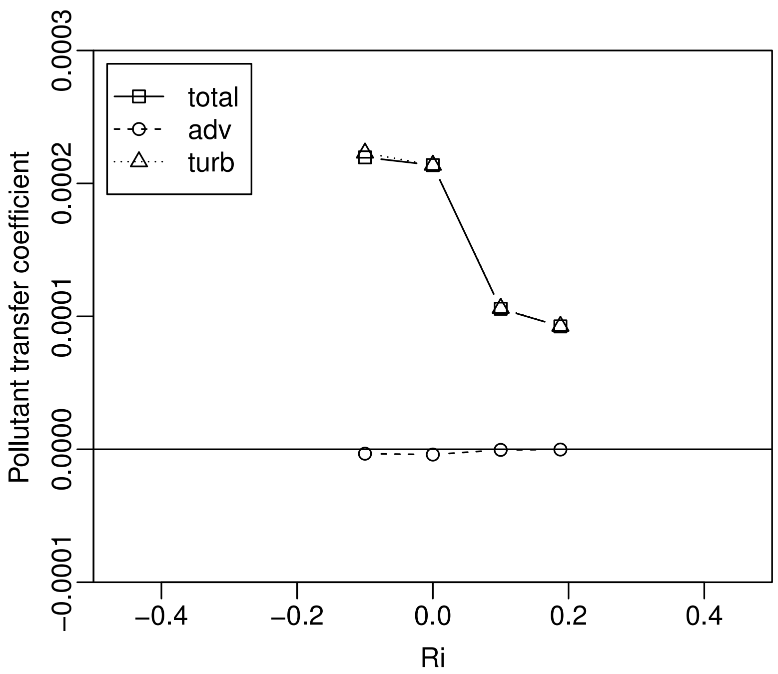

(b)

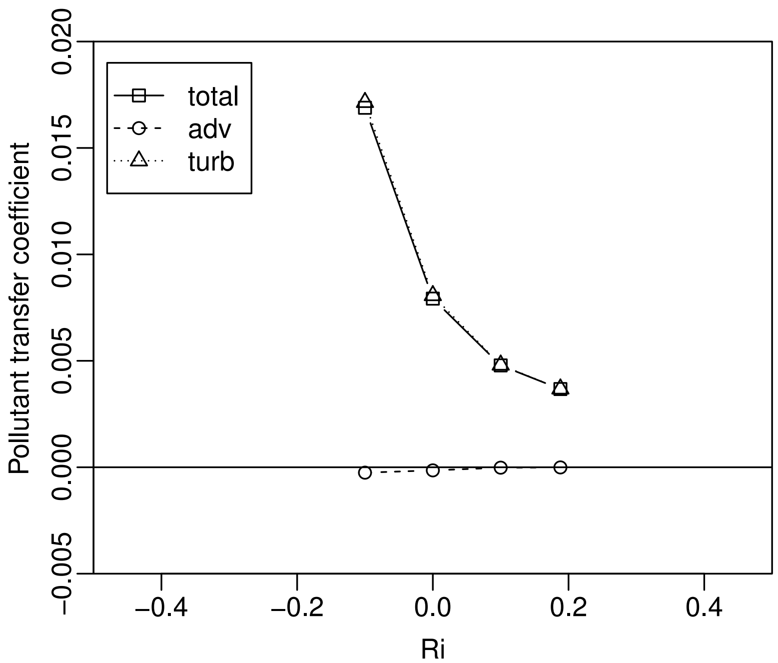

Figure 13: The normalized pollutant (passive, line scalar source) transfer coefficients by mean flow, turbulence, and in total between the RSL and (a) the street ground Φ_{B0}; (b) the canyon air Φ_{BC} under different stratifications.

(a)

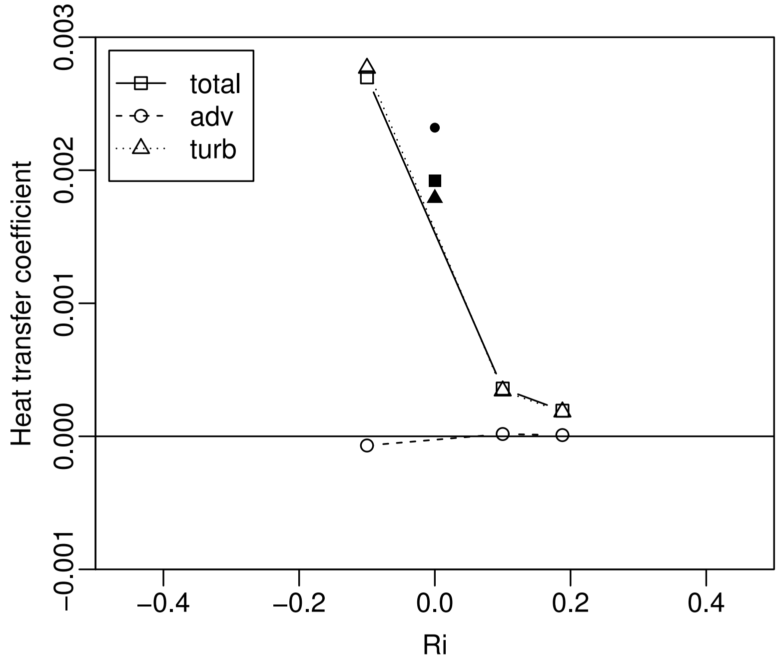

(b)

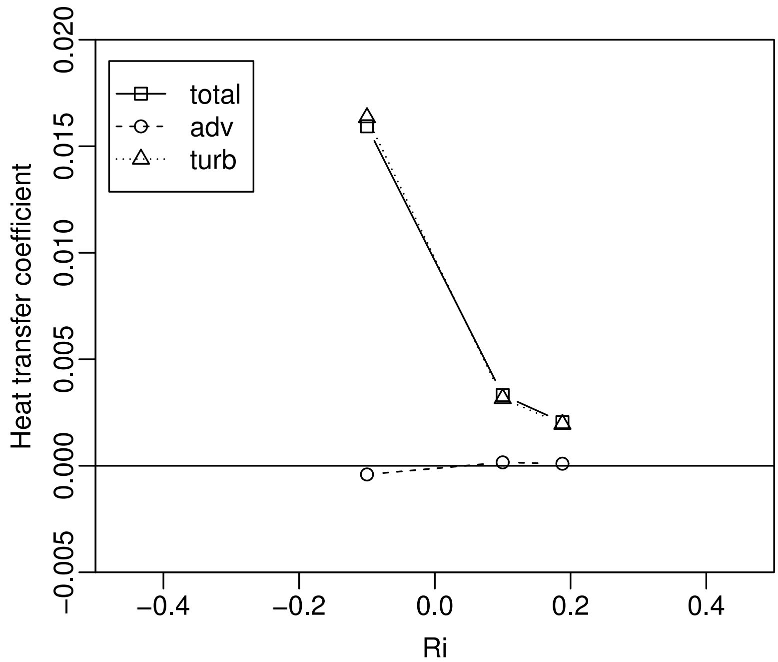

Figure 14: The normalized heat (active, area scalar source) transfer coefficients by mean flow, turbulence, and in total between the RSL and (a) the street ground Φ_{B0}; (b) the canyon air Φ_{BC} under different stratifications. Also shown are the transfer coefficient of a passive scalar (area source) under neutral stratification (Ri = 0) from wind tunnel (Barlow et al., 2004): filled square; LES (Cai et al., 2008): filled triangle; and LES (Cheng and Liu, 2011a): filled circle.